Comparative study of neutron irradiation and carbon doping in MgB_2 single crystals

C. Krutzler,[1] M. Zehetmayer,[1] M. Eisterer,[1,*] H. W. Weber,[1] N. D. Zhigadlo,[2] and J. Karpinski[2]
[1]*Atomic Institute of the Austrian Universities, 1020 Vienna, Austria*
[2]*Solid State Physics Laboratory, ETH, 8093 Zurich, Switzerland*
(Received 22 December 2006; revised manuscript received 28 February 2007; published 19 June 2007)

We compare the reversible and irreversible magnetic properties of superconducting carbon doped and undoped MgB_2 single crystals before and after neutron irradiation. A large number of samples with transition temperatures between 38.3 and 22.8 K allows us to study the effects of disorder systematically. Striking similarities are found in the modification of the reversible parameters by irradiation and doping, which are discussed in terms of impurity scattering and changes of the Fermi surface. The irreversible properties are influenced by two counteracting mechanisms: they are enhanced by the newly introduced pinning centers but degraded by changes in the thermodynamic properties. Accordingly, the large neutron induced defects and the small defects from carbon doping lead to significantly different effects on the irreversible properties. Finally, the fishtail effect caused by all kinds of disorder is discussed in terms of an order-disorder transition of the flux-line lattice.

DOI: 10.1103/PhysRevB.75.224510 PACS number(s): 74.70.Ad, 74.25.Ha, 74.62.Dh, 61.80.Hg

I. INTRODUCTION

A lot of effort has been invested since the discovery of superconductivity in MgB_2,[1] in order to improve its superconducting properties for possible applications. Strong pinning and high upper critical fields are needed for applications, such as high field magnets. It was shown[2] for polycrystalline MgB_2 that the small upper critical field for fields parallel to the crystallographic c axis $[\mu_0 H_{c2}^c(0) \approx 3\ \mathrm{T}]$ limits the application range of MgB_2. At this field, the first grains (grains with their boron plane oriented perpendicular to the applied field) of an untextured tape or wire become normal conducting. At higher fields, the critical currents are strongly suppressed and only small percolative supercurrents prevail. As for several materials in the past, doping and particle irradiation turned out to be appropriate methods for improving the upper critical field or pinning and for investigating changes of the superconducting properties in a systematic way. Among the numerous possibilities of doping MgB_2, carbon seems to be most promising for enhancing H_{c2}. Carbon substitutes boron in the MgB_2 crystal structure.[3] Neutron irradiation was found to increase not only the upper critical field but also pinning. By irradiating doped crystals, it is possible to combine both methods in one crystal.

Intensive research efforts over the past years have clarified many aspects of the mechanism of superconductivity in MgB_2, for a review, see Ref. 4. *S*-wave pairing caused by electron-phonon coupling was established soon and the Fermi surface was found to consist of four energy bands. Two of them originate from the in-plane orbitals of the boron atoms and are denoted as σ bands. These bands have a cylindrical shape and are strongly anisotropic. On the other hand, the boron p_z orbitals forming the π bands are more isotropic. Today, it is experimentally and theoretically established that the anisotropic shape of the Fermi surface together with an anisotropic electron-phonon coupling on the different sheets of this Fermi surface leads to two energy gaps of different sizes. The gap in the π bands, Δ_π, is about 2 meV, whereas the gap in the σ bands, Δ_σ, is about 7 meV due to the strong coupling of the electrons to the E_{2g} phonon mode. Considering the nearly equal density of states (DOS) of these different bands at the Fermi level, this results in the two-band behavior of MgB_2. Interband coupling is sufficiently weak to avoid substantial smearing of the two-band effects but is still responsible for a common closing of both energy gaps at the same temperature in zero field. Thus, many superconducting properties of MgB_2 can be successfully described by a simple two-band model[5,6] with two spherical Fermi surfaces for the π and the σ band (in particular, for $H \| c$). For anisotropic properties such as H_{c2}, other models were chosen for the Fermi surface topology,[7,8] or different diffusivities along the main crystallographic directions were introduced in dirty limit models.[9,10] The introduction of point defects in such a system modifies the upper critical field by both inter- and intraband scattering, potentially increasing the upper critical field but decreasing the transition temperature.

In this article, we report on investigations of the magnetic properties of several carbon doped and undoped MgB_2 single crystals before and after neutron irradiation. Section II provides some details of the experiments including the measurement and evaluation methods, carbon doping (Sec. II A), and neutron irradiation (Sec. II B). The results will be presented and discussed in Sec. III. Particular emphasis is placed on the systematic effects by introducing disorder. We start with a comparison of the reversible properties (transition temperature, upper critical fields, and anisotropy) in Sec. III A and discuss them in terms of the two-band model in MgB_2. Then (Sec. III A), the irreversible properties (magnetization loops and critical current density) are analyzed with respect to the different kinds of defects introduced by different treatments (i.e., by carbon doping or neutron irradiation) and under the consideration of their effects on the reversible properties. The second peak, which emerges in all samples when introducing disorder, is discussed in terms of an order-disorder transition. Finally, we provide a summary and conclusions in Sec. IV.

TABLE I. Transition temperature T_c of differently doped $Mg(B_{1-x}C_x)_2$ single crystals before and after each irradiation step. δT_c denotes the decrease of the transition temperature after irradiation in undoped samples (0%) and the temperature difference to 38.3 K in carbon doped samples. ΔT_c denotes the superconducting transition width. F_N refers to the fast neutron fluence for samples irradiated in the central irradiation facility and to the thermal neutron fluence (*) for samples irradiated with a soft neutron spectrum.

Carbon	F_N (10^{21} m^{-2})	T_c (K)	$-\delta T_c$ (K)	ΔT_c (K)
0%	0	38.3	—	0.15
0%	0.1	38.2	0.1	0.17
0%	2	37.3	1	0.22
0%	4	36.55	1.8	0.33
0%	10	34.1	3.9	0.44
0%	0.15*	35.75	2.6	1.6
0%	0.8*	30.45	7.75	1.6
0%	1.2*	26.55	11.6	2.4
0%	1.6*	22.8	15.35	3
3.8%	0	35.4	2.8	2.4
3.8%	2	34.7	3.5	2.54
6.6%	0	33.15	5.05	4.0
6.6%	2	32.0	6.2	4.3
6.6%	4	31.35	6.85	4.5
9.5%	0	30.5	7.7	7.0

II. EXPERIMENT

All single crystals investigated in this study were grown at the Solid State Laboratory ETH-Zurich using a high-pressure technique in a cubic anvil press. Details concerning the undoped samples can be found in Ref. 11 and concerning the carbon doped samples $[Mg(B_{1-x}C_x)_2]$ in Ref. 12. The typical size of the single crystals is about 0.3–1 mm in the basal plane (parallel to the boron planes of MgB_2) and 0.02–0.2 mm along the c direction (parallel to the uniaxial axis of MgB_2).

The magnetic measurements in fields up to 8 T were performed in a noncommercial superconducting quantum interference device (SQUID) magnetometer (for more experimental details, see Refs. 13 and 14), a 7 T SQUID magnetometer (Quantum Design), and a 5 T vibrating sample magnetometer. The transition temperature T_c (Table I) was obtained from ac susceptibility measured in a commercial 1 T SQUID magnetometer (Quantum Design) with a special low field option. The applied ac-field amplitude was 30 μT and the onset of a tangent criterion was used to evaluate T_c. Here, the steepest slope in the transition of the in-phase susceptibility was linearly extrapolated to zero magnetization and the intersection point of the tangent with the x axis used to define T_c. The transition width ΔT_c is defined by the drop of the in-phase susceptibility from 10% to 90% of the Meissner signal. The increase of the transition width after fast neutron irradiation is rather small (0.1–0.3 K), indicating the homogeneity of the radiation-induced defect structure, whereas larger changes were found upon thermal neutron irradiation. The magnetization measurements at fixed field or fixed temperature were used to define the upper critical fields (H_{c2}^c for $H\|c$ and H_{c2}^{ab} for $H\|ab$) as the field or temperature, where the magnetic moment (m) vanishes. The corresponding anisotropy is calculated via $\gamma=H_{c2}^{ab}/H_{c2}^c$. Further details are available in Refs. 15 and 16.

The critical current density parallel to the ab planes (J_c) can be calculated from the hysteresis width of the magnetic moment (m) in increasing (H_+) and decreasing field (H_-) employing an extended Bean model. Assuming a constant absolute value of the critical current density in the sample, the general definition of the magnetic moment induced by a current distribution $\vec{m}_i=0.5\int d^3r\vec{r}\times\vec{J}_c$ directly leads to $J_c(B)=\{m_i(B)/V\}\{4/[b(1-b/3a)]\}$ $(a\geqslant b)$ for rectangularly shaped crystals, $m_i(H)=0.5[m(H_-)-m(H_+)]$ denotes the irreversible magnetic moment in the c direction, and $V=abc$ is the sample volume, where a and b are the sample lengths parallel to the ab plane, and c in the c direction. The small field correction due to the current induced stray field H_s is numerically calculated leading to the magnetic induction $B=\mu_0(H+H_s)$.

A. Carbon doping

The effects of doping on MgB_2 can be summarized as follows (see, for example, Ref. 12 and references therein): The carbon atoms substitute boron at the boron lattice sites (defining the crystallographic ab plane) and thereby enhance impurity scattering due to lattice distortions in the boron sublattice by chemical disorder. Generally, the defects introduced by doping presumably act as point defects.[17] In the two-band superconductor MgB_2, at least three different scattering rates have to be considered:[18] intraband scattering within the π and σ bands and interband scattering between π and σ bands. It was argued that the retention of two-band superconductivity supports the conclusion that interband scattering is hardly influenced by doping—at least up to a carbon content of 10% ($x=0.1$). Higher doping concentrations are discussed controversially.[19–23] Thus, it is most likely that intraband scattering increases, but it is still under discussion which of the energy bands is affected more.[18,24–26] Several studies have shown an increase in H_{c2} in polycrystalline materials[3,27,28] as well as in single crystals,[12,24,29,30] which can be related to increased intraband scattering. A second important effect of carbon substitution is electron doping by the additional electron provided by the carbon atom. According to band structure calculations[31] and electron energy-loss spectroscopy experiments,[32] electron doping mainly affects the holes in the σ bands which are continuously filled. This results in a shift of the Fermi level, making the Fermi surface more isotropic. Therefore, carbon doping was also found to reduce the anisotropy in MgB_2 due to a decrease of the σ band anisotropy.[12,24,29,30,33]

B. Neutron irradiation

Neutron irradiation introduces defects in MgB_2 mainly by the neutron capture reaction of ^{10}B. The resulting reaction

products (^{7}Li ions and alpha particles) create the defects. Defects resulting from direct collisions of fast neutrons with lattice atoms seem to be negligible. The size of the defects ranges from several nanometers (i.e., similar to the coherence length) supported by transmission electron microscopy investigations down to pointlike defects.[34,35] For further details concerning the irradiation of MgB_2, see Refs. 36 and 37.

Neutron irradiation was performed in the TRIGA-MARK-II research reactor in Vienna. Most samples were irradiated in the central irradiation facility with a fast/thermal flux density of $7.6/6.1\times10^{16}$ m^{-2} s^{-1}. Fast neutrons are defined by $E>0.1$ MeV, thermal neutrons by $E<0.55$ eV.[38] Only two samples were irradiated in a position outside the graphite reflector, with a rather soft neutron spectrum (fast/thermal flux density: $1.4/30\times10^{14}$ m^{-2} s^{-1}). The large cross section for the neutron capture of ^{10}B at low neutron energy leads to a larger defect density in the surface regions compared to the interior of the material, even in single crystals. The transition width increased significantly (up to 3 K for a decrease of T_c by approximately 16 K) in these two crystals. Therefore, the thermal neutrons were shielded with a cadmium foil in the central irradiation facility, in order to achieve a more homogeneous defect distribution over the entire sample volume as indicated by a small superconducting transition width ΔT_c (see Table I). Note that also in that case, defects are mainly introduced by the neutron capture reaction.[36]

The irradiation of pure MgB_2 leads to comparable results in both positions,[35] which supports the conclusion, that mainly the neutron capture reaction is responsible for the observed modifications since the fast neutron fluence differs by orders of magnitude (see also Ref. 37). It is rather difficult to calculate the number of neutron capture reactions, since the neutron spectrum has to be known accurately and geometry dependent self-shielding effects have to be taken into account. Such calculations were performed for larger bulk samples irradiated in the central irradiation facility.[36] We did not repeat these calculations for the actual crystal geometries or for the second irradiation facility, since the defect concentration, which results from one neutron capture reaction, is unknown. In any case, the defect concentration is proportional to the neutron fluence, although with different proportionality constants. Since the neutron capture cross section is largest at low neutron energies, we refer to the thermal fluence for samples irradiated without cadmium screen. The fast neutron fluence is given for all other samples, since the low energy neutrons are absorbed in the cadmium shield. Since the transition temperature decreases linearly (see Sec. III) with defect concentration, we introduce this decrease ($-\delta T_c$) as "disorder parameter," which is proportional to the defect density. We find that a thermal fluence of 4×10^{20} m^{-2} in the position outside the reflector induces the same number of defects as a fast neutron fluence of 10^{22} m^{-2} in the central irradiation facility (with cadmium screen).

III. RESULTS AND DISCUSSION

A. Reversible properties

Table I summarizes the transition temperature and the width of the superconducting transition before and after each irradiation step for all samples of this study.

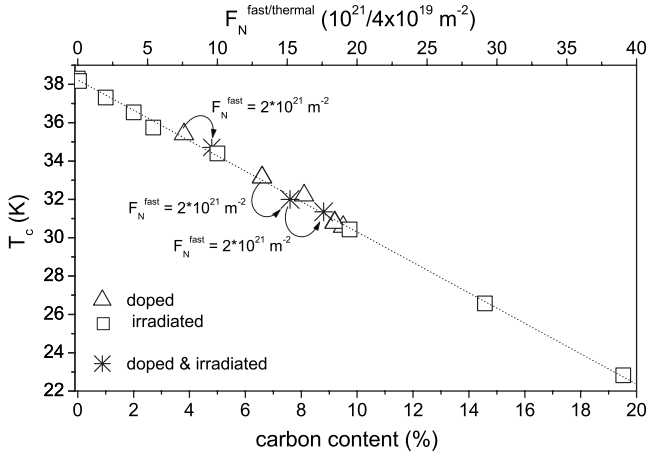

FIG. 1. Transition temperature T_c of irradiated doped, irradiated pure, and unirradiated doped MgB_2 as a function of carbon content and fast neutron fluence. The arrows indicate the irradiation steps of the doped crystals; the dotted line is a guide to the eyes. 1% carbon doping corresponds to a fast/thermal neutron fluence of $2\times10^{21}/8\times10^{19}$ m^{-2}, respectively.

Figure 1 shows the transition temperature of several MgB_2 single crystals as a function of doping and irradiation. For doping (carbon content less than 10%) as well as for neutron irradiation, a linear decrease of T_c is found in agreement with reports in the literature.[12,35] If we associate 1% carbon doping with $F_N^{\text{fast}}=2\times10^{21}$ m^{-2} and with $F_N^{\text{thermal}}=8\times10^{19}$ m^{-2}, we find that all data collapse on a common straight line. For doped irradiated crystals (stars in Fig. 1), we added the neutron fluence to the carbon content, as indicated by the arrows. Thus, the disorder parameter $-\delta T_c$, which was introduced in Sec. II B to quantify neutron induced disorder, can be extended to disorder introduced by carbon doping by $\delta T_c=38.3\text{ K}-T_c$. Although this seems rather arbitrary at this point, since the transition temperature might be reduced by different mechanisms, it turns out to be very useful for the comparison of the reversible properties.

Two main mechanisms are responsible for the reduction of T_c. First, a decrease of the DOS at the Fermi level, and, second, interband scattering. Carbon doping adds additional electrons to the system, which fills the bands, shifts the Fermi level, and thus reduces the DOS. According to theoretical calculations, this seems to be enough to explain the experimentally observed reduction of T_c.[19] Also, disorder can reduce the DOS by smearing the Fermi surface.[39] A reduction of the DOS following irradiation was proposed for MgB_2 (Refs. 17, 40, and 41) and observed by NMR in neutron irradiated MgB_2 with a T_c of 7 K.[42]

For interband scattering, a saturation of T_c is predicted at approximately 25–22 K,[6,19,43,44] where the σ and the π gap are predicted to merge. This gap merging was reported for both neutron irradiated[45] and for carbon doped[20] MgB_2, although at lower temperatures than predicted. No saturation was observed. The transition temperature decreases continuously and nearly linearly with increasing defect density down to 7 K in irradiation experiments with He ions[40] or with neutrons.[37,46] For highly carbon doped samples ($\gtrsim$10%), the decrease of the transition temperature becomes

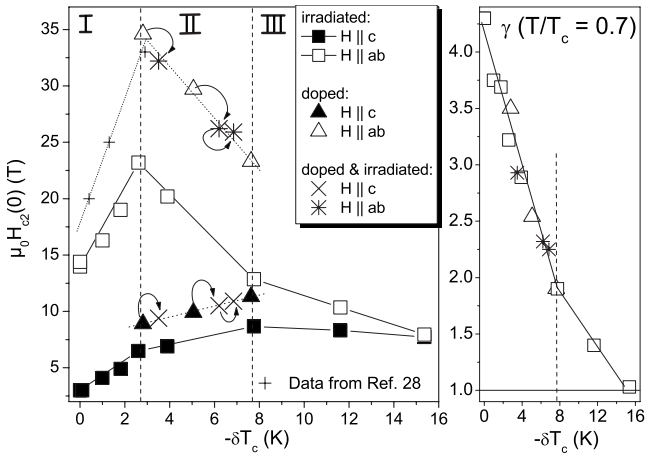

FIG. 2. Reversible parameters of MgB_2 with defects from doping and neutron irradiation as a function of $-\delta T_c$. The point at $-\delta T_c=0$ refers by definition to a typical undoped, unirradiated sample. The left panel shows the upper critical fields at zero temperature, $H_{c2}(0)$, for $H\|c$ and $H\|ab$. The anisotropy evaluated from H_{c2} at $T/T_c=0.7$ is plotted in the panel at the right-hand side. Data for low carbon substitution (+ symbols) are taken from Ref. 28 and the lines are guides to the eyes. The arrows indicate irradiation steps of 2×10^{21} m^{-2}.

even faster.[12] In both cases, interband scattering alone cannot explain the behavior of T_c and an additional reduction of the DOS has to be considered. Note that in the case of carbon doping, not all studies report gap merging,[47,48] which makes the role of interband scattering in carbon doped samples even more controversial.

Figure 2 shows some reversible parameters evaluated on doped and irradiated MgB_2. The left panel presents the upper critical fields extrapolated to zero temperature, $H_{c2}(0)$, as a function of $-\delta T_c$ for $H\|c$ (H_{c2}^c, full symbols) and $H\|ab$ (H_{c2}^{ab}, open symbols). Using this abscissa instead of the transition temperature T_c has the further advantage that $-\delta T_c$—in contrast to T_c—increases with the defect density. The values for the transition temperature itself can be obtained from $-\delta T_c$ by taking $T_c=38.3$ K as the transition temperature of typical undoped as-grown MgB_2 single crystals. Data for low doping levels are taken from investigations on carbon doped MgB_2 filaments in Ref. 28.

Generally, doping as well as irradiation increase the upper critical field, the enhancement being larger for doping. Three different regions can be separated in the dependence of $H_{c2}(0)$ on $-\delta T_c$ which are indicated by the vertical dashed lines in Fig. 2. In region I, which refers to low defect densities, we find increasing upper critical fields with increasing defect density for both field orientations. We find a nearly linear increase of the upper critical field with increasing defect concentration, as expected from the Gor'kov-Goodman relation,[49,50] which is based on impurity scattering. Note that we do not have own data for carbon doping in this region and use data from literature[28] for $H\|ab$. We are not aware of any available data for $H\|c$ in this doping and T_c regime. In principle, H_{c2} is affected by intra- and interband scattering, but since T_c is not changed very much in this region, interband scattering must be much smaller and is negligible for the reduction of the mean free path of the charge carriers. For a given mean free path (or H_{c2}), the transition temperature is more reduced in the neutron irradiated samples. This indicates a higher interband scattering rate in these samples, since the other mechanism (reduction of the DOS) reducing the transition temperature should be more pronounced for doping. Charge doping only occurs in doped samples and the reduction of the DOS due to disorder is expected to be the same in doped and irradiated samples, since it is induced by the same parameter as the increase of H_{c2} itself, i.e., the intraband scattering rate in the σ band. This is consistent with the calculations of Ref. 41, where a negligible reduction of the DOS was reported at small levels of disorder and interband scattering found to be responsible for the decrease of T_c at low neutron fluences.

A common behavior is observed in region II. We again observe a linear dependence of $H_{c2}(-\delta T_c)$ with the same slope (within experimental accuracy) in the irradiated and doped samples and even in the irradiated doped samples. The decrease of $H_{c2}^{ab}(-\delta T_c)$ is about 2.2 T/K and the increase of $H_{c2}^{c}(-\delta T_c)$ about 0.5 T/K. It is rather striking that doping and irradiation modify the properties, responsible for changes in H_{c2} and T_c, in the same way in region II, since only smearing of the DOS and a decrease of the mean free path are directly correlated with each other, while charge doping is absent in undoped samples and interband scattering seems to be weaker in the doped samples, at least in region I. Since there is no reason why interband scattering should not be further increased in the neutron irradiated samples and the saturation of T_c is predicted at much lower temperatures, either interband scattering in carbon doped samples becomes more important in region II or the influence of charge doping in carbon substituted samples compensates the stronger reduction of T_c in the irradiated samples. Another unexpected and interesting fact is that doped and irradiated samples enter region II at the same value of $-\delta T_c\approx2.8$ K ($T_c\approx35.4$ K), which corresponds to 3.8% carbon doping and $F_N^{fast}=7.6\times10^{21}$ m^{-2}, respectively. At this point, H_{c2}^{ab} has a maximum and the slope changes rapidly so that H_{c2}^{ab} decreases in region II, whereas H_{c2}^{c} of the irradiated samples changes its slope but still increases in region II. It is difficult to explain this behavior, because none of other fundamental parameters, as for instance, the lattice parameters, the energy gaps, the reduction of the DOS, or the transition temperature, show such abrupt changes at $-\delta T_c\approx2.8$ K. Intraband scattering cannot be responsible for this abrupt change since it is different in doped and undoped samples at this point, as indicated by the different upper critical fields. Note that the decrease of T_c cannot explain the reduction of the upper critical field (for $H\|ab$) alone since extrapolation leads to zero H_{c2} well above zero transition temperature.

At high defect densities in region III ($-\delta T_c\gtrsim8$ K, $T_c\lesssim30.2$ K), only data on irradiated crystals are available. H_{c2} decreases with increasing defect density for both field orientations, the decrease of H_{c2}^{ab} being flatter than in region II.

The right-hand panel in Fig. 2 shows the anisotropy evaluated from the upper critical fields for the experimentally accessible region of the phase diagram at $T/T_c=0.7$ as a function of $-\delta T_c$. The anisotropy of irradiated doped MgB_2

follows the common trend found for unirradiated doped and irradiated pure MgB_2 as a function of $-\delta T_c$ as a consequence of the upper critical field behavior. Further, only two regions in the dependence of the anisotropy on the defect density are separated, regions I and II in the upper critical field dependence show the same (linear) behavior in the anisotropy. As already mentioned in Sec. II A, the decrease of anisotropy in the case of carbon doping is usually related to band filling, which results in a more isotropic σ band, whereas scattering has to be responsible for the decrease of anisotropy in the case of neutron irradiation. The similar dependence of the anisotropy on $-\delta T_c$ for doping and irradiation could again indicate that the same mechanism is responsible in both cases (i.e., scattering—and not band filling in the case of doping). Another possibility is that the decrease of the anisotropy itself is (at least partly) responsible for the reduced transition temperature.[51–53]

High fluence irradiation experiments show that MgB_2 becomes isotropic when T_c is reduced by approximately 16 K (T_c=22.8 K). At such defect densities, two energy gaps have still been detected.[45] Thus, the σ band has already become isotropic at these defect densities or the anisotropy is reduced by an increasing importance of the nearly isotropic π band.

Summarizing the changes in the reversible parameters by doping, irradiation, and also by a combination of both, we find that the introduction of both kinds of defect structures influences these parameters in a similar way as a function of the defect density expressed by $-\delta T_c$, which most likely indicates the number of small defects (scattering centers). Since scattering seems to be responsible for all changes, we find no clear traces of the predicted influence of charge doping on T_c or on the upper critical field anisotropy, although the reduction in the DOS due to charge doping might (partly) compensate the higher interband scattering rate in neutron irradiated samples, leading to a similar reduction of T_c.

B. Irreversible properties

Figure 3 shows magnetization loops of an irradiated carbon doped (3.8% carbon content, $F_N^{fast}=2\times10^{21}$ m^{-2}) MgB_2 single crystal at several temperatures for $H\|c$. Similar curves were observed on all other irradiated samples (Ref. 34 and Fig. 4). The most striking effect of neutron irradiation is the emergence of a pronounced fishtail effect over a large temperature interval in all investigated samples. No fishtail was observed in any unirradiated *undoped* sample and only small effects in unirradiated *doped* ones. At low defect density, the fishtail is observed only near H_{c2}, whereas large parts of the magnetization loops remain reversible. With increasing defect density (i.e., increasing $-\delta T_c$), the effect is extended to lower (reduced) fields and the hysteresis width becomes larger, but the fishtail behavior goes through a maximum and becomes again less pronounced at very high defect densities.

These effects are demonstrated in Fig. 4, where loop measurements at around 5 K are compared for doped and undoped MgB_2 before and after neutron irradiation. To make the results independent of sample size or geometry, we replace the usually quoted magnetization $M=m/V$ (V denotes the sample volume) by αM, where $\alpha=4/[b(1-b/3a)]$ (a and

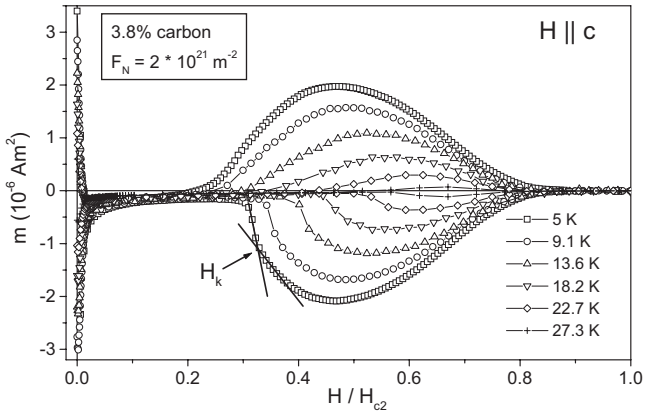

FIG. 3. Magnetization loops of an irradiated doped MgB_2 single crystal for fields along the c axis at several temperatures. The kink field H_k, which refers to the order-disorder transition field of the flux-line lattice, is indicated by the intersection point of two lines in the 5 K curve.

b are the lengths of the rectangular sample in the ab plane). Note that α comes from the calculation of J_c in rectangular samples according to the Bean model, i.e., $J_c(H)=|M(H)|\alpha$, if the reversible magnetization is neglected (see Sec. II). Thus, the hysteresis width obtained from αM at increasing and decreasing fields is proportional to J_c ($\sim 2J_c$) and therefore independent of sample geometry. Furthermore, these loops were measured at the same reduced temperature T/T_c, with T=5 K for the unirradiated pure sample, whereas the temperature is slightly adjusted in all other samples, so that $T/T_c \simeq 5/38.3$.

Concentrating at first only on the undoped samples in Fig. 4 (curve 0), we see that most of $M(H)$ in the unirradiated state lies in the reversible regime even at 5 K indicating a poor as-grown defect structure. This is significantly changed upon neutron irradiation even at the very low fast neutron fluence of only 1×10^{20} m^{-2} ($-\delta T_c \simeq 0.1$ K, curve 1). We find larger J_c at low fields, a larger (first) irreversibility field [the lowest field where $m(H)$ becomes reversible], and a fishtail effect near H_{c2}. These observations make very effective radiation-induced pinning centers plausible, as suggested in Ref. 34, i.e., defects with a radius of about 5 nm which is only slightly smaller than the coherence length in MgB_2 of $\sim$10 nm at low temperatures.[15] It also justifies disregarding the preirradiation defect structure as pinning centers. While the curves at low fluences (0, 1) are still reversible over a large part of the field range, they become irreversible from 0 T to almost H_{c2} at a higher fluence level, see the results at $F_N^{fast} \simeq 2\times10^{21}$ m^{-2} ($-\delta T_c \simeq 1.0$ K) in Fig. 4 (curve 2). Additionally, the hysteresis width near the second peak field is strongly enhanced. At very high defect density ($-\delta T_c \simeq 15.4$ K, $F_N^{therm} \simeq 1.6\times10^{21}$ m^{-2}, curve 3), the MgB_2 crystal is still irreversible over almost the whole field range, but the maximum hysteresis width (i.e., J_c) is significantly smaller than for $-\delta T_c \simeq 1.0$ K. As mentioned before, we presume that the fast and the thermal neutron irradiation create a very similar defect structure at the same $-\delta T_c$ due to the same defect creation mechanism (see Sec. II B), which is strongly supported by the results in the overlapping $-\delta T_c$ range (crys-

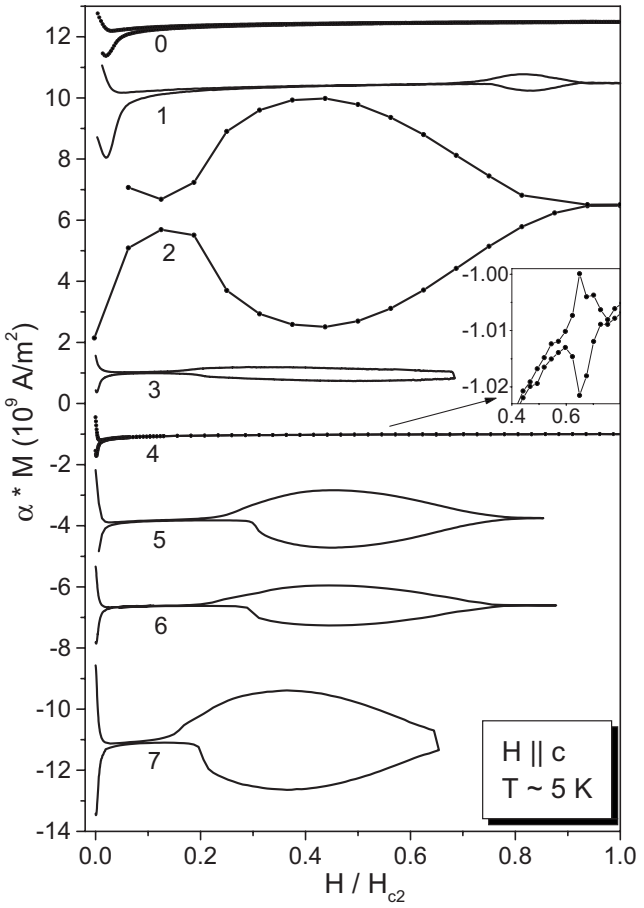

FIG. 4. Comparison of magnetization loops modified by defects introduced by doping and irradiation for $H\|c$ at $T\sim 5$ K ($T/T_c \simeq 5/38.3$). Each curve is shifted by a constant value along the vertical axis for clarity. The magnetization M is modified by the factor α, so that $J_c(H)\simeq|M(H)|\alpha$, i.e., the hysteresis width equals about $2J_c$ (see text). The numbers refer to (0) undoped unirradiated sample; (1) undoped, $-\delta T_c\simeq 0.1$ K, $F_N^{fast}\simeq 0.1\times 10^{21}$ m^{-2}; (2) undoped, $-\delta T_c\simeq 1.0$ K, $F_N^{fast}\simeq 2\times 10^{21}$ m^{-2}; (3) undoped, $-\delta T_c\simeq 15.4$ K, $F_N^{therm}\simeq 1.6\times 10^{21}$ m^{-2}; (4) carbon content $x=3.8\%$, $-\delta T_c\simeq 2.9$ K; (5) $x=3.8\%$, $-\delta T_c\simeq 3.6$ K, $F_N^{fast}\simeq 2\times 10^{21}$ m^{-2}; (6) $x=6.6\%$, $-\delta T_c\simeq 6.3$ K, $F_N^{fast}\simeq 2\times 10^{21}$ m^{-2}; and (7) $x=6.6\%$, $-\delta T_c\simeq 7.0$ K, $F_N^{fast}\simeq 4\times 10^{21}$ m^{-2}.

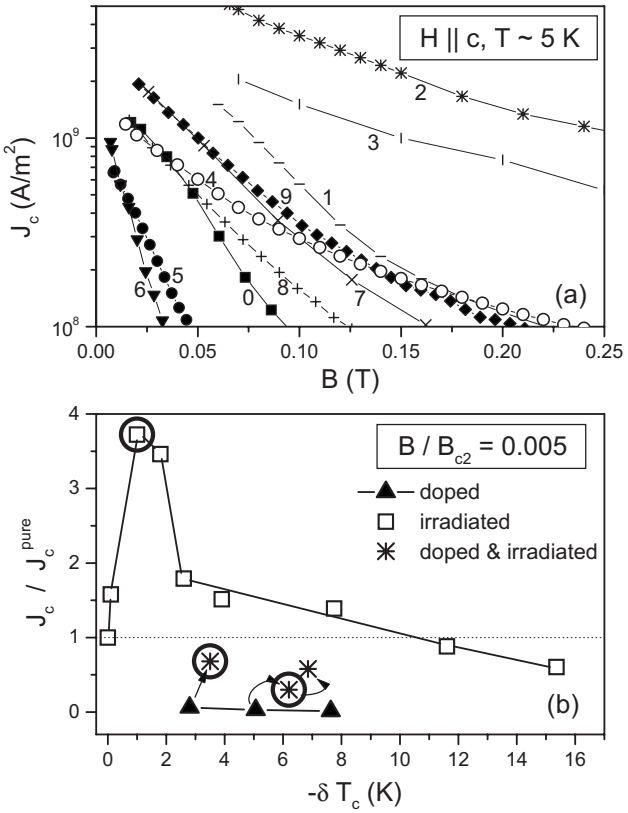

FIG. 5. Panel (a) $J_c(B)$ at low fields. The numbers refer to (0) undoped unirradiated sample; (1): undoped, $-\delta T_c\simeq 0.1$ K, $F_N^{fast}\simeq 0.1\times 10^{21}$ m^{-2}; (2) undoped, $-\delta T_c\simeq 1.0$ K, $F_N^{fast}\simeq 2\times 10^{21}$ m^{-2}; (3) undoped, $-\delta T_c\simeq 3.9$ K, $F_N^{fast}\simeq 10\times 10^{21}$ m^{-2}; (4) undoped, $-\delta T_c\simeq 15.4$ K, $F_N^{therm}\simeq 1.6\times 10^{21}$ m^{-2}; (5) carbon content $x=3.8\%$, $-\delta T_c\simeq 2.9$ K; (6) $x=9.5\%$, $-\delta T_c\simeq 7.7$ K; (7) $x=3.8\%$, $-\delta T_c\simeq 3.6$ K, $F_N^{fast}\simeq 2\times 10^{21}$ m^{-2}; (8) $x=6.6\%$, $-\delta T_c\simeq 6.3$ K, $F_N^{fast}\simeq 2\times 10^{21}$ m^{-2}; and (9) $x=6.6\%$, $-\delta T_c\simeq 7.0$ K, $F_N^{fast}\simeq 4\times 10^{21}$ m^{-2}. Panel (b) Critical current density normalized to J_c of pure MgB_2 as a function of $-\delta T_c$ ($0.0\text{ K}\leqslant -\delta T_c\leqslant 15.4$ K) at the reduced field $B/B_{c2}=0.005$ and $T\sim 5$ K ($T/T_c\simeq 5/38.3$). Most of the results refer to direct measurements; only some of them were obtained by extrapolation from slightly higher fields. Each arrow indicates a fast neutron fluence step of 2×10^{21} m^{-2}; the dotted line refers to $J_c/J_c^{pure}=1$. The encircled symbols highlight the results for $F_N^{fast}=2\times 10^{21}$ m^{-2}.

tals with $-\delta T_c$ between 0.1 and 3.9 K are available from fast neutron irradiation, and between 2.6 and 15.4 K from thermal neutron irradiation), where good correspondence was found for the reversible and for the irreversible properties.

The changes of the hysteresis width at the second peak field with increasing $-\delta T_c$ are qualitatively similar to the behavior at low fields, as illustrated in Fig. 5, where $J_c(B)$ is shown in panel (a) and the enhancement of J_c at very low reduced fields ($B/B_{c2}\simeq 0.005$) with respect to the unirradiated undoped sample (J_c^{pure}) in panel (b) ($H\|c$, $T/T_c \simeq 5/38.3$). Note that there is some sample-to-sample variation in J_c^{pure}, which could slightly change the results of panel (b). With increasing $-\delta T_c$, J_c starts to grow rapidly but reaches a rather sharp maximum of about $4J_c^{pure}$ [at $B/B_{c2}\simeq 0.005$, panel (b)] at $-\delta T_c\sim 1-2$ K, then drops significantly to about $2J_c^{pure}$ at $-\delta T_c\sim 2.5$ K, and finally decreases more smoothly and linearly to values below those in the as-grown samples, i.e., to about $0.5J_c^{pure}$ at $-\delta T_c\sim 15.4$ K. Qualitatively, similar results are found at other low fields [panel (a)].

This behavior suggests that neutron irradiation influences the irreversible properties of MgB_2 by different counteracting mechanisms. It is obvious that the addition of pinning centers (i.e., defects) enhances the pinning properties, which is considered the main reason for the large increase of J_c at low $-\delta T_c$. At the same time, disorder also modifies the reversible properties as shown in the previous section, which control the pinning force, the elasticity of the flux-line lattice, etc. For instance, when the upper critical field grows, the coherence length decreases and therefore the pinning volume is reduced. It was also shown[15] that the critical field

decreases with increasing $-\delta T_c$ (at least at low $-\delta T_c$) which reduces at the same time the condensation energy for flux-line pinning, whereas a reduction of the anisotropy makes the flux-line lattice stiffer,[54] which lowers its ability to adapt to the defect matrix. More quantitative statements are difficult because of a lack of experimental data at higher defect densities. While the coherence length (ξ_{ab}) is easily obtained from the upper critical field via the Ginzburg Landau relations [e.g., $B_{c2}^c=\Phi_0/(2\pi\xi_{ab}^2)$, $\Phi_0\simeq 2.07\times 10^{-15}$ V s], the magnetic penetration depths (and other properties calculated from the Ginzburg Landau relations) are assessed by fitting the reversible magnetization, whose accessibility becomes more difficult at higher defect densities since the irreversible fraction of the curves grows. In addition, we have to consider that the low field results for J_c call for a two-band description, but the low field properties are even less well established at high defect densities.[15] It should be realized, however, that the behavior of J_c is qualitatively similar at high fields (e.g., at the peak field), where the behavior is mainly controlled by the σ band properties.[15] We also note that the rapid decline of J_c between about $-\delta T_c\sim 2$ and 2.5 K approximately correlates with the crossover from regions I to II in Fig. 2, which indicates some significant changes in the reversible properties there.

Turning now to the carbon doped samples in Fig. 4 (curve 4) and Fig. 5 (curves 5 and 6), we find a small fishtail even in the unirradiated crystals (inset in Fig. 4), which becomes slightly more pronounced with increasing carbon doping. At very low reduced fields ($B/B_{c2}\simeq 0.005$), however, the critical current density degrades [Fig. 5(b)] to $J_c/J_c^{pure}\simeq 0.06$ at $x=3.8\%$, 0.03 at $x=6.6\%$, and 0.01 at $x=9.5\%$. We point out that the changes are less dramatic when going to lower reduced fields (e.g., $J_c/J_c^{pure}\simeq 0.3$ at $x=9.5\%$ and $B/B_{c2}\simeq 0.002$) or when comparing J_c at nonreduced fields. The latter is shown in Fig. 5(a), where we observe that the main effect of carbon doping is a significant enhancement of the slope of J_c vs B (at low fields) and a corresponding reduction of the irreversibility field. The opposite behavior is usually observed in carbon doped bulks[55,56] or films.[57] The grain boundaries are the dominant pinning centers in these materials and the irreversibility field as well as the field dependence of J_c are determined only by the upper critical field.[2,58] The irreversibility field is given by $H_{c2}^{ab}/\sqrt{p_c^2(\gamma^2-1)+1}$ in untextured MgB_2. Thus, the increase of the upper critical field and the reduction of the anisotropy enhance the irreversibility fields and consequently reduce the field dependence of J_c. The fishtail observed in single crystals actually indicates the emergence of new defects from doping. However, these defects are presumably very small and therefore only weak pinning centers, the corresponding improvement of pinning being obviously counteracted by the reversible properties. Indeed, as shown in Fig. 2 and Ref. 16, the differences in the reversible properties of doped and undoped samples are very significant, and all changes, i.e., higher upper critical fields, lower condensation energy, and anisotropy in the carbon doped samples, lead to worse pinning properties.

Irradiation of the carbon doped samples (by fast neutrons) leads to similar effects as in undoped samples, i.e., the fishtail becomes quite pronounced and J_c at low fields increases strongly. For instance, at a carbon doping level of 3.8%, a fast neutron fluence of 2×10^{21} m^{-2} enhances J_c at low fields by a factor of about 11 ($B/B_{c2}\simeq 0.005$). The resulting $J_c(B)$ is larger than $J_c^{pure}(B)$ [Fig. 5(a)] but smaller at not too low reduced fields [Fig. 5(b)]. At a carbon doping level of 6.6%, J_c also increases significantly upon the second irradiation step from 2 to 4×10^{21} m^{-2} but also remains below J_c^{pure} in the representation of Fig. 5(b). The results suggest again that the preirradiation defects can be neglected as pinning centers, thus making the pinning matrices similar in doped and undoped irradiated single crystals. Note that Figs. 4 and 5 include results on three different samples at $F_N^{fast}\simeq 2\times 10^{21}$ m^{-2} [see encircled symbols in Fig. 5(b)], an undoped one (i.e., $x=0\%$), and two doped ones ($x=3.8\%$ and 6.6%, respectively), which should provide (almost) the same defect structure for flux-line pinning. The strong differences in J_c, e.g., $J_c^{x=0}:J_c^{x=3.6\%}:J_c^{x=6.6\%}\simeq 12:2:1$ at $B/B_{c2}\simeq 0.005$, where J_c^x refers to the critical current density of a sample with carbon content x, accordingly reflect the changes in the reversible properties and their significant influence on flux-line pinning (which is obviously worsening with increasing $-\delta T_c$) directly.

The fishtail effect in a superconductor can be ascribed to an order-disorder transition of the vortex matter. According to this widely accepted interpretation (e.g., Ref. 59 and references therein), the flux-line lattice changes from an ordered state at low fields, mainly controlled by vortex interactions, to a disordered state at higher fields, where the vortex-defect interaction dominates. In the disordered state, the lattice is better adjusted to the pinning matrix, leading to a higher J_c, which explains nicely the second peak. The exact field of the transition is often associated with the kink field evaluated in increasing fields,[60] H_k (see arrow in Fig. 3), which will also be used in this work, but the onset field (i.e., the minimum between first and second peaks) shows very similar values and temperature dependencies.[34] It was recently shown that the temperature dependence of H_k in both neutron irradiated undoped single crystals[34] and in unirradiated carbon doped crystals[61] matches calculations of the order-disorder transition according to Ref. 59, when assuming δl *pinning* (i.e., pinning due to variations in the mean free path[62]).

Figure 6 shows the reduced kink-field H_k/H_{c2}^c as a function of $-\delta T_c$ (0.1 K$\leqslant -\delta T_c\leqslant$15.4 K, note that pure samples do not exhibit a second peak) at 0 K (extrapolated from the low temperature values). Considering only the undoped irradiated samples (squares in Fig. 6), $-\delta T_c$ is proportional to the defect density (n_d) of the large defects responsible for the fishtail. With growing defect density, we find that $H_k/H_{c2}^c(0)$ decreases rapidly at low $-\delta T_c$ ($-\delta T_c\lesssim 2$ K), then goes trough a minimum between about 4 and 8 K and increases at high $-\delta T_c$. This corresponds to the field range of the fishtail, discussed above, which emerges only near H_{c2} at low fluences (i.e., low $-\delta T_c$), but moves to significantly lower fields at higher fluences. In terms of the order-disorder transition, H_k/H_{c2}^c is expected to reflect the pinning properties, i.e., strong flux-line pinning would shift the order-disorder transition to lower fields (and vice versa, see Ref. 59 for details). Accordingly, we expect a qualitative correlation with the

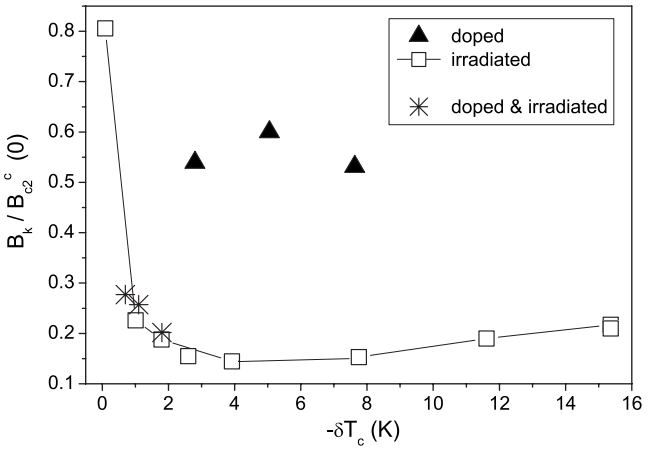

FIG. 6. Order-disorder transition field H_k normalized by the upper critical field at 0 K as a function of $-\delta T_c$ ($0.1\ \mathrm{K} \leqslant -\delta T_c \leqslant 15.4\ \mathrm{K}$) for defects resulting from doping and irradiation. Note that $-\delta T_c$ refers to the reduction of T_c by irradiation only in the case of the irradiated doped samples in this figure.

critical current density, which is indeed observed when comparing Figs. 6 and 5 (i.e., a large J_c tends to reveal a low H_k and vice versa). Both curves go through an extreme value, but the maximum of J_c rather corresponds to the flattening of H_k. In principle, a growing defect density improves pinning, i.e., H_k/H_{c2}^c should decrease, but disorder also modifies the reversible properties of the superconductor, which in turn influences H_k. According to the theory,[59] H_k/H_{c2}^c increases when the anisotropy or H_{c2} decreases (at constant defect density). As shown in Fig. 2, in fact, both γ and H_{c2} are reduced at very high $-\delta T_c$ providing a possible explanation of the increase of H_k/H_{c2}^c there.

Unirradiated carbon doped MgB_2 single crystals exhibit small traces of a fishtail at intermediate fields; thus, H_k/H_{c2}^c vs $-\delta T_c$ is much higher than in the irradiated samples (Fig. 6), reflecting much weaker pinning properties in correspondence with the low J_c values shown in Fig. 5. Note that the evaluation of H_k suffers from some uncertainties due to the small magnetic moment of these samples. It appears reasonable to assume that the defect density corresponds directly to the carbon boron substitution, i.e., a carbon content of 1% would induce a defect density of about $7 \times 10^{26}\ \mathrm{m}^{-3}$ (calculated using the size of a unit cell[12]), which increases linearly with x. Applying this defect density, the theoretical calculations of the order-disorder transition field[59] lead to agreement with the experimental H_k when employing a defect radius of about 0.25 nm, which is close to the size of a unit cell.

Neutron irradiation strongly affects the irreversible properties of the carbon doped samples, which justifies neglecting the pinning matrix of the preirradiated samples for flux-line pinning. Thus, we expect a similar H_k/H_{c2}^c vs $-\delta T_c$ dependence as in undoped irradiated samples if we redefine $-\delta T_c$ to refer only to the reduction of T_c caused by irradiation (i.e., with respect to T_c of the unirradiated doped sample in the case of doped samples). This is indeed observed (Fig. 6). The somewhat larger values in the carbon doped samples can be ascribed to differences in the reversible properties, e.g., to the smaller anisotropy. We note, however, that the influence of the reversible properties on H_k is much less pronounced than on J_c.

IV. SUMMARY AND CONCLUSION

The modification of the reversible and irreversible properties in irradiated and/or doped MgB_2 is determined by the particular introduced defect structure. Pointlike defects from doping and also from irradiation are found to act similarly on the reversible parameters of MgB_2. Contrary, the modification of the pinning matrix is dominated by larger defects only introduced by neutron irradiation. Both kinds of defects act independently in irradiated doped MgB_2 single crystals. The superconducting properties show the same dependence on neutron fluence in doped and undoped crystals and the same dependence on carbon content in unirradiated and irradiated MgB_2. No additional features are found by combining both methods of influencing the superconducting parameters in one sample.

The similar behavior of the reversible properties of MgB_2, such as the upper critical field and the transition temperature, with increasing carbon substitution and neutron fluence is rather unexpected, since the predicted influence of charge doping should only occur in the case of carbon doping. Scattering seems to be the dominant mechanism in both cases, increasing the upper critical field and reducing the transition temperature in both kinds of samples. We find evidence for higher interband scattering rates in neutron irradiated samples at low levels of disorder, leading to the same H_{c2} at a smaller T_c. At higher levels of disorder, further changes of the reversible properties become nearly identical. This can be caused either by an enhancement of interband scattering in carbon doped samples or stronger interband scattering in irradiated samples compensates a reduction in the DOS by charge doping in the case of carbon substituted samples. The presently available theoretical models are insufficient for a complete and consistent explanation of the dependence of the reversible parameters on the defect densities introduced by doping and irradiation. Our results seem to justify further theoretical work, e.g., by including the σ band anisotropy in the existing two-band model.

Introducing disorder in MgB_2 essentially influences the irreversible properties by two counteracting mechanisms. The changes in the reversible parameters mainly deteriorate the pinning properties with increasing disorder, whereas at the same time, the number of pinning centers grows, which of course improves pinning. Carbon doping introduces only small pinning centers. Therefore, the negative effects coming from the reversible properties dominate at all doping levels. Neutron irradiation induces much larger (i.e., more efficient) pinning centers, which results in a strong enhancement of the irreversible properties at intermediate defect densities and at low fields and in the emergence of a pronounced fishtail effect at higher fields indicating an order-disorder transition of the flux-line lattice. At high defect density, the impact of the reversible parameters begins to dominate and J_c significantly decreases. In neutron irradiated doped samples, the pinning matrix is also dominated by the efficient radiation-induced defects, which enhance the irreversible properties

with respect to the unirradiated doped sample similarly as in undoped samples, but the combined influence of doping and irradiation on the reversible properties leads to a J_c value at low fields, which remains significantly lower than in undoped samples at the same fluence.

ACKNOWLEDGMENTS

The authors thank H. Hartmann for technical assistance. This work has been supported by the Swiss National Science Foundation through NCCR MaNEP.

*eisterer@ati.ac.at

[1] J. Nagamatsu, N. Nakagawa, T. Muranaka, Y. Zenitani, and J. Akimitsu, Nature (London) **410**, 63 (2001).
[2] M. Eisterer, C. Krutzler, and H. W. Weber, J. Appl. Phys. **98**, 033906 (2005).
[3] R. A. Ribeiro, S. L. Budko, C. Petrovic, and P. C. Canfield, Physica C **384**, 227 (2003).
[4] Physica C **385**, 1 (2003).
[5] E. J. Nicol and J. P. Carbotte, Phys. Rev. B **71**, 054501 (2005).
[6] O. V. Dolgov, R. K. Kremer, J. Kortus, A. A. Golubov, and S. V. Shulga, Phys. Rev. B **72**, 024504 (2005).
[7] T. Dahm and N. Schopohl, Phys. Rev. Lett. **91**, 017001 (2003).
[8] M. Mansor and J. P. Carbotte, Phys. Rev. B **72**, 024538 (2005).
[9] A. Gurevich, Phys. Rev. B **67**, 184515 (2003).
[10] A. A. Golubov and A. E. Koshelev, Phys. Rev. B **68**, 104503 (2003).
[11] J. Karpinski, S. M. Kazakov, J. Jun, M. Angst, R. Puzniak, A. Wisniewski, and P. Bordet, Physica C **385**, 42 (2003).
[12] S. M. Kazakov, R. Puzniak, K. Rogacki, A. V. Mironov, N. D. Zhigadlo, J. Jun, C. Soltmann, B. Batlogg, and J. Karpinski, Phys. Rev. B **71**, 024533 (2005).
[13] M. Zehetmayer, F. M. Sauerzopf, J. Karpinski, M. Murakami, and H. W. Weber, Physica C **383**, 232 (2002).
[14] F. M. Sauerzopf, Phys. Rev. B **57**, 10959 (1998).
[15] M. Zehetmayer, M. Eisterer, J. Jun, S. M. Kazakov, J. Karpinski, and H. W. Weber, Phys. Rev. B **70**, 214516 (2004).
[16] C. Krutzler, M. Zehetmayer, M. Eisterer, H. W. Weber, N. D. Zhigadlo, J. Karpinski, and A. Wisniewski, Phys. Rev. B **74**, 144511 (2006).
[17] R. H. T. Wilke, S. L. Bud'ko, P. C. Canfield, J. Farmer, and S. T. Hannahs, Phys. Rev. B **73**, 134512 (2006).
[18] I. I. Mazin, O. K. Andersen, O. Jepsen, O. V. Dolgov, J. Kortus, A. A. Golubov, A. B. Kuzmenko, and D. van der Marel, Phys. Rev. Lett. **89**, 107002 (2002).
[19] J. Kortus, O. V. Dolgov, R. K. Kremer, and A. A. Golubov, Phys. Rev. Lett. **94**, 027002 (2005).
[20] R. S. Gonnelli, D. Daghero, A. Calzolari, G. A. Ummarino, V. Dellarocca, V. A. Stepanov, S. M. Kazakov, N. Zhigadlo, and J. Karpinski, Phys. Rev. B **71**, 060503(R) (2005).
[21] Z. Holanova, P. Szabo, P. Samuely, R. H. T. Wilke, S. L. Budko, and P. C. Canfield, Phys. Rev. B **70**, 064520(R) (2004).
[22] G. A. Ummarino, D. Daghero, R. S. Gonnelli, and A. H. Moudden, Phys. Rev. B **71**, 134511 (2005).
[23] H. Schmidt, K. E. Gray, D. G. Hinks, J. F. Zasadzinski, M. Avdeev, J. D. Jorgensen, and J. C. Burley, Phys. Rev. B **68**, 060508(R) (2003).
[24] M. Angst, S. L. Budko, R. H. T. Wilke, and P. C. Canfield, Phys. Rev. B **71**, 144512 (2005).
[25] A. V. Sologubenko, N. D. Zhigadlo, S. M. Kazakov, J. Karpinski, and H. R. Ott, Phys. Rev. B **71**, 020501(R) (2005).
[26] I. Pallecchi, V. Braccini, E. G. dAgliano, M. Monni, A. S. Siri, P. Manfrinetti, A. Palenzona, and M. Putti, Phys. Rev. B **71**, 104519 (2005).
[27] Z. Holova, J. Kacmarcik, P. Szabo, P. Samuely, I. Sheikin, R. A. Ribeiro, S. L. Budko, and P. C. Canfield, Physica C **404**, 195 (2004).
[28] R. H. T. Wilke, S. L. Budko, P. C. Canfield, D. K. Finnemore, R. J. Suplinskas, and S. T. Hannahs, Phys. Rev. Lett. **92**, 217003 (2004).
[29] T. Masui, S. Lee, A. Yamamoto, H. Uchiyama, and S. Tajima, Physica C **412**, 303 (2004).
[30] T. Masui, S. Lee, and S. Tajima, Phys. Rev. B **70**, 024504 (2004).
[31] N. I. Medvedeva, A. L. Ivanovskii, J. E. Medvedeva, and A. J. Freeman, Phys. Rev. B **64**, 020502(R) (2001).
[32] R. F. Klie, J. C. Zheng, Y. Zhu, A. J. Zambano, and L. D. Cooley, Phys. Rev. B **73**, 014513 (2006).
[33] S. Lee, T. Masui, A. Yamamoto, H. Uchiyama, and S. Tajima, Physica C **397**, 7 (2003).
[34] M. Zehetmayer, M. Eisterer, J. Jun, S. M. Kazakov, J. Karpinski, B. Birajdar, O. Eibl, and H. W. Weber, Phys. Rev. B **69**, 054510 (2004).
[35] M. Eisterer, Phys. Status Solidi C **2**, 1606 (2005).
[36] M. Eisterer, M. Zehetmayer, S. Toenies, H. W. Weber, M. Kambara, N. H. Babu, D. A. Cardwell, and L. R. Greenwood, Supercond. Sci. Technol. **15**, L9 (2002).
[37] C. Tarantini *et al.*, Phys. Rev. B **73**, 134518 (2006).
[38] H. W. Weber, H. Böck, E. Unfried, and L. R. Greenwood, J. Nucl. Mater. **137**, 236 (1986).
[39] L. R. Testardi and L. F. Mattheiss, Phys. Rev. Lett. **41**, 1612 (1978).
[40] R. Gandikota *et al.*, Appl. Phys. Lett. **86**, 012508 (2005).
[41] M. Putti, P. Brotto, M. Monni, E. Galleani, A. Sanna, and S. Massidda, Europhys. Lett. **77**, 57005 (2007).
[42] A. P. Gerashenko, K. N. Mikhalev, S. V. Verkhovskii, A. E. Karkin, and B. N. Goshchitskii, Phys. Rev. B **65**, 132506 (2002).
[43] A. Y. Liu, I. I. Mazin, and J. Kortus, Phys. Rev. Lett. **87**, 087005 (2001).
[44] S. C. Erwin and I. I. Mazin, Phys. Rev. B **68**, 132505 (2003).
[45] M. Putti, M. Affronte, C. Ferdeghini, P. Manfrinetti, C. Tarantini, and E. Lehmann, Phys. Rev. Lett. **96**, 077003 (2006).
[46] M. Putti *et al.*, Appl. Phys. Lett. **86**, 112503 (2005).
[47] H. Schmidt, K. E. Gray, D. G. Hinks, J. F. Zasadzinski, M. Avdeev, J. D. Jorgensen, and J. C. Burley, Phys. Rev. B **68**, 060508(R) (2003).
[48] P. Samuely, P. Szabo, P. C. Canfield, and S. L. Budko, Phys. Rev. Lett. **95**, 099701 (2005).
[49] B. B. Goodman, IBM J. Res. Dev. **6**, 63 (1962).
[50] M. Eisterer, R. Müller, R. Schöppl, H. W. Weber, S. Soltanian, and S. X. Dou, Supercond. Sci. Technol. **20**, 117 (2007).
[51] M. Zehetmayer, H. W. Weber, and E. Schachinger, J. Low Temp.

Phys. **133**, 407 (2003).
[52] T. Schneider and D. DiCastro, Phys. Rev. B **72**, 054501 (2005).
[53] S. Ruiz-Chavarria, G. Tavizon, and P. de la Mora, J. Phys.: Condens. Matter **18**, 1403 (2006).
[54] E. H. Brandt, Rep. Prog. Phys. **58**, 1465 (1995).
[55] R. H. T. Wilke, S. L. Bud ko, P. C. Canfield, M. J. Kramer, Y. Q. Wu, D. K. Finnemore, R. J. Suplinskas, J. V. Marzik, and S. T. Hannahs, Physica C **424**, 1 (2005).
[56] S. X. Dou *et al.*, Phys. Rev. Lett. **98**, 097002 (2007).
[57] A. V. Pogrebnyakov *et al.*, Appl. Phys. Lett. **85**, 2017 (2004).
[58] M. Eisterer, M. Zehetmayer, and H. W. Weber, Phys. Rev. Lett. **90**, 247002 (2003).
[59] G. P. Mikitik and E. H. Brandt, Phys. Rev. B **64**, 184514 (2001).
[60] K. K. Uprety, J. Horvat, X. L. Wang, M. Ionescu, H. K. Liu, S. X. Dou, and E. H. Brandt, Phys. Rev. B **65**, 224501 (2002).
[61] E. Ohmichi, E. Komatsu, T. Masui, S. Lee, S. Tajima, and T. Osada, Phys. Rev. B **70**, 174513 (2004).
[62] G. Blatter, M. V. Feigel'man, V. B. Geshkenbein, A. I. Larkin, and V. M. Vinokur, Rev. Mod. Phys. **66**, 1125 (1994).